ANNALS OF GEOPHYSICS, 67, 6, S655, 2024; doi:10.4401/ag-8980
OPEN ACCESS

Comparisons and characteristics of site amplifications using noise and earthquake data: Examples from the Malta Seismic Network

Daniela Farrugia[*,1], Pauline Galea[1], Sebastiano D'Amico[1]

(1) Department of Geosciences, University of Malta

Article history: received December 5, 2023; accepted November 7, 2024

Abstract

In the past decade, numerous studies on the amplification effects due to the local geology have been conducted in the Maltese islands (Central Mediterranean). Due to the lack of permanent seismic stations on geological areas of concern, ambient noise techniques were utilised. The areas of interest are characterised by clay, that can reach a thickness of 75 m, buried beneath limestone which introduces a velocity inversion in the stratigraphy. With the expansion of the Malta Seismic Network (MSN) to three stations in such zones, the possibility of confirming and further investigating the results using empirical data arises. Here we present results, using 3 years of data including time-domain and frequency-domain analysis in terms of Standard Spectral Ratio (SSR) and earthquake H/V. In particular, we note that the amplifications obtained using the SSR technique are significantly higher than those obtained using both noise and earthquake H/V techniques. Additional peaks below 1 Hz of significant amplitude are also obtained on the SSR curves. By separating the earthquake data set on the basis of distance from the islands, we show that this amplification is source-dependent, and that the high amplification values originate from larger, more distant earthquakes in the Hellenic arc.

Keywords: Site effects; Amplification; Horizontal-to-Vertical Spectral ratio; Malta Seismic Network; Standard spectral ratio

1. Introduction

Historical evidence has shown how, in the event of an earthquake, soft soil sites have suffered significantly greater damage than rock sites. Evidence of the significance and complexity of site effects has been observed from events including Loma Prieta 1989 (M6.9, California, US, Mizuno and Abe, 1991), Kocaeli and Duzce 1999 (M7.4 and M7.2 respectively, Turkey, Rathje et al., 2006), Chi-Chi 1999 (M7.6, Taiwan, Rathje et al., 2005), Christchurch 2011 (Dellow et al., 2011), Nepal 2015 (Takai et al., 2016) etc.

Site effects can be estimated by means of numerical simulations and experimental methods (Pilz et al., 2009). Popular experimental methods include the Standard Spectral Ratio (SSR) and the Horizontal-to-Vertical Spectral Ratio (H/V) technique (Parolai, 2012). The SSR method consists of computing the ratio of the Fourier amplitude spectra of earthquake recordings at the target site to that on a nearby rock (reference) site while the H/V method

involves the recording of ambient noise or earthquake recordings at the target site and computing the ratio of the horizontal to the vertical spectra. Since the SSR requires two stations (one on the target site and one on the reference site) and the recordings of numerous earthquakes, it is not the ideal method for a quick estimate of site response (Foti et al., 2011). For this reason, the H/V method has been widely used to study site effects of both shallow and deep sedimentary structures (Cornou et al., 2003; Bonnefoy-Claudet et al., 2006).

Comparison of site responses obtained with reference (SSR) and non-reference site techniques (H/V) has shown that while the fundamental resonance frequency of a site is consistently estimated by both methods, the H/V technique usually underestimates the level of amplification (e.g. Field and Jacob, 1995; Bonilla et al., 1997; Riepl et al., 1998; Parolai et al., 2012).

The geology of the Maltese islands (Central Mediterranean, Fig. 1) is characterised by a four-layer sequence of limestones and clays. Starting from the bottom and oldest, these are: the Lower Coralline Limestone (LCL), the Globigerina Limestone (GL), the Blue Clay (BC) and the Upper Coralline Limestone (UCL) (refer to Fig. 1). A common feature found in the western half of the archipelago is Upper Coralline Limestone plateaus and hillcaps covering a soft Blue Clay layer which can be up to 75 m thick. This introduces a velocity inversion in the stratigraphy. Even though the islands lie in an area with a level of background seismicity that is low to moderate, and generally not perceived as of high risk, historically rare damaging events have occurred. Galea (2007) compiled a historical catalogue of felt earthquakes on Malta since 1530, based on historical documents or instrumental seismicity parameters. Since 1530, at least four earthquakes of intensity VII on the European Macroseismic Scale (EMS-98) were experienced. The source region which historically appears to generate the largest felt effects in the region is SE Sicily. Large events occurring in the Hellenic Arc have also produced significant damage on the islands. Despite the large distance, a magnitude 7.7 earthquake in 1856, with an epicentral location around 1000 km away from the islands, caused significant damage to buildings, with many houses suffering serious cracks to their walls. This makes it important to consider far-field events when considering seismic hazard. Figure 2 displays the epicentral location of the earthquakes that produced an intensity of at least VI experienced on the islands.

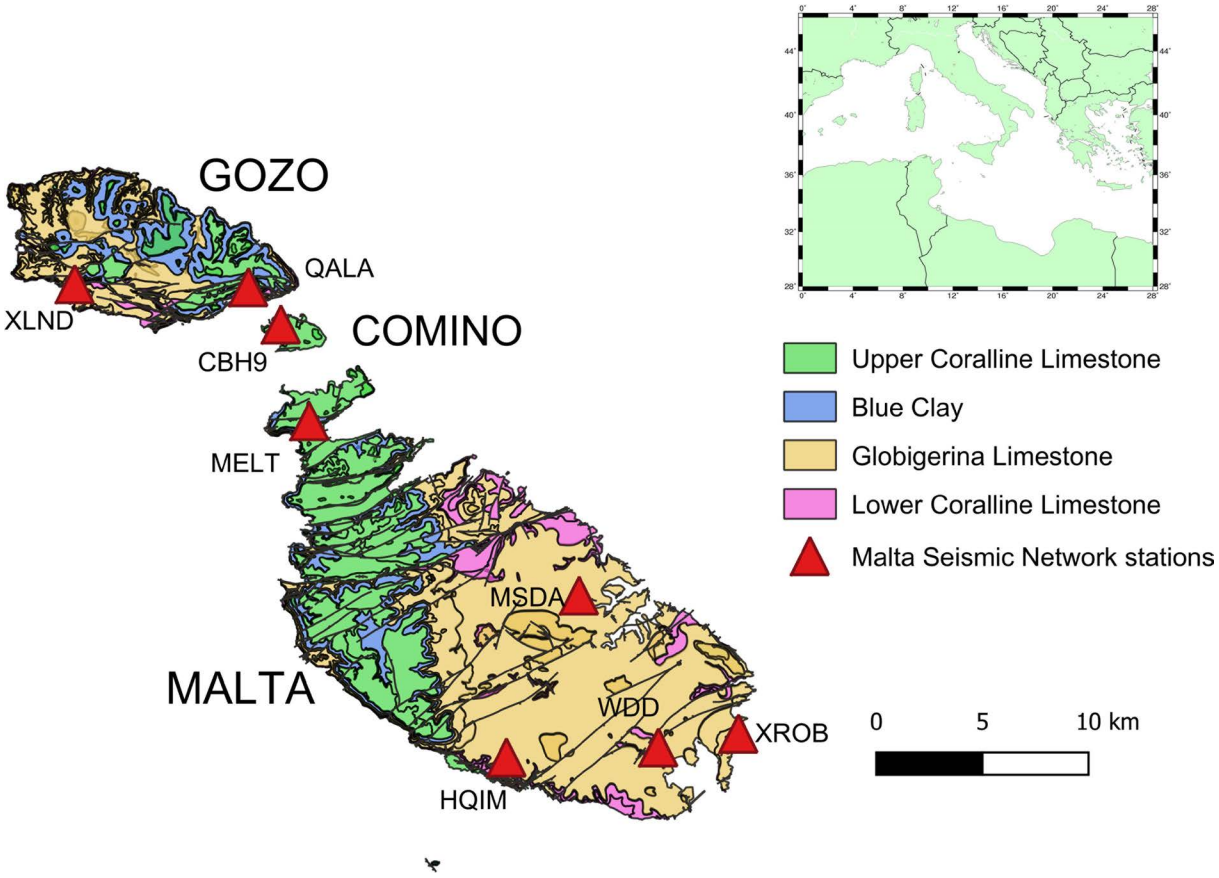

Figure 1. Geological map of the Maltese islands. The red triangles represent the stations of the Malta Seismic Network. Inset shows the location of the Maltese islands in the Mediterranean Sea.

In the past decade, effort has been made in understanding better the local site effects. Studies have been carried out both on a national scale, as well as in the form of microzonation studies in some areas of the archipelago. These studies, through the recording of ambient seismic noise and analysis of horizontal-to-vertical spectral ratios (H/V), have revealed that areas where the clay layer is present within the lithostratigraphy, have the clear potential to amplify ground motion in specific frequency ranges, as opposed to the eastern half of the archipelago which is not characterised by any soft material of significant thickness (Panzera et al., 2013; Vella et al., 2013). The local seismic response in regions of the Maltese islands characterised by the low-velocity clay layer buried underneath limestone, was also evaluated using the equivalent linear numerical code SHAKE2000 in Farrugia et al. (2020). These results have important implications for the prediction of building behaviour.

Through participation in national and European funded projects, in particular the INTERREG Italia-Malta programmes, the Malta Seismic Network (MSN) was built up over a 6-year period, with the acquisition of a number of 3-component broad-band stations (Fig. 1). At the time of writing, the MSN comprises eight stations covering the three major islands of the Maltese archipelago – Malta, Gozo and Comino. It is managed by the Seismic Monitoring and Research Group (SMRG) within the Department of Geosciences, University of Malta, and is the only seismic network on the islands, thus serving as the national network. The Malta Seismic Network is registered with the code ML with the Federation of Digital Seismic Networks (FDSN) (Galea et al., 2021).

With the extension of the MSN to sites underlain by clay, local site response analysis using earthquake data was now possible. In this study we use earthquake and noise recordings made by the MSN to provide a deeper understanding of site effects on the islands. Analyses include the comparison of seismograms both in time and in frequency domain and also the comparison of three different methods for obtaining site responses: H/V from earthquake recordings and from microtremors and the Standard Spectral Ratio technique.

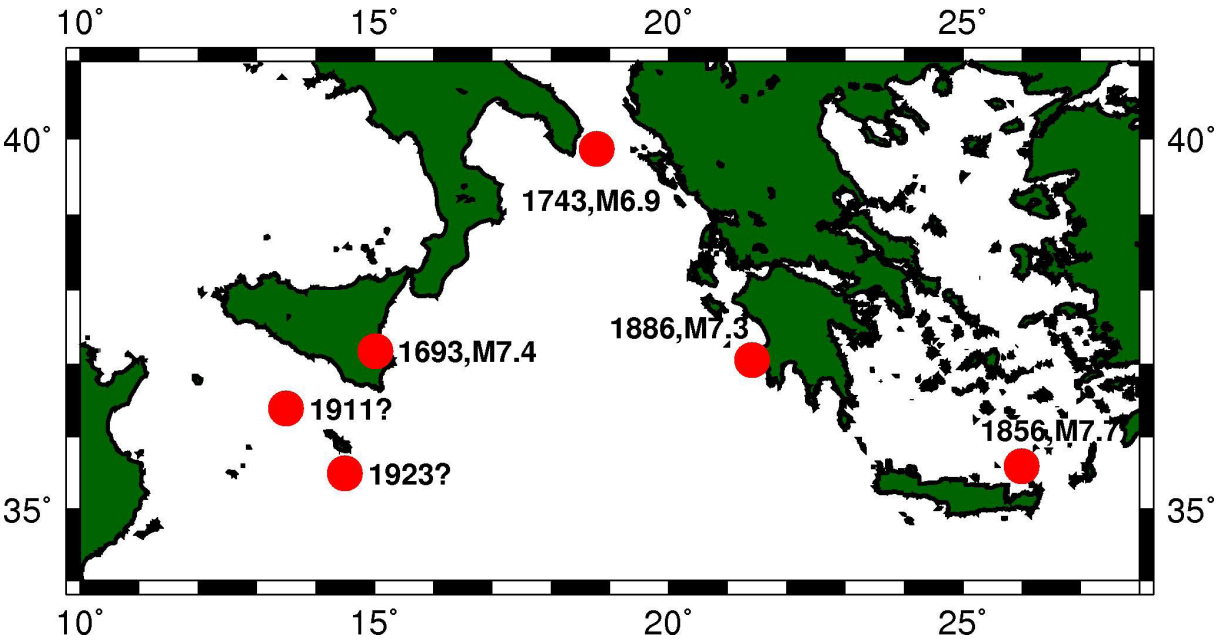

Figure 2. Location of earthquakes that caused damage of intensity ≥ VI since 1500 (modified from (Vella et al., 2013)).

2. The Malta Seismic Network

The MSN currently comprises eight 3-component stations distributed over the three main islands of the Maltese Archipelago: Malta, Gozo and Comino. Figure 1 shows the present configuration of the network and Table 1 lists the coordinates and technical information on each station.

The first installed station was WDD, which was the only station available from 1995 till 2014. It lies inside a tunnel on the Lower Coralline Limestone, the oldest and hardest layer of the sedimentary sequence. XLND, which is found in Gozo, also lies on the LCL. MSDA is installed on the Lower GL while MELT, CBH9 and QALA all lie on the UCL formation. Shear-wave velocity profiles were obtained near the MELT and CBH9 stations, using surface

Station Name	Latitude	Longitude	Elevation (m)	Geology	Instrument
CBH9	36.01	14.33	27	UCL	Trillium compact (120 s-100 Hz); Centaur digitizer (Nanometrics)
HQIM	35.83	14.44	129	GL	GeoTINY (10 s-120 Hz)
MELT	35.97	14.34	98	UCL	Trillium compact (120 s-100 Hz); Centaur digitizer
MSDA	35.90	14.48	48	GL	Trillium 120PA (120 s-100 Hz); Centaur digitizer
QALA	36.03	14.31	103	UCL	Trillium compact (120 s-100 Hz); Centaur digitizer
WDD	35.84	14.52	22	LCL	STS-2 (120 s-50 Hz), Quanterra Q330
XLND	36.03	14.22	31	LCL	Trillium 120PA (120 s-100 Hz); Centaur digitizer
XROB	35.84	14.57	31	GL	Trillium compact (120 s-100 Hz); Centaur digitizer

Table 1. Information about the stations of the Malta Seismic Network.

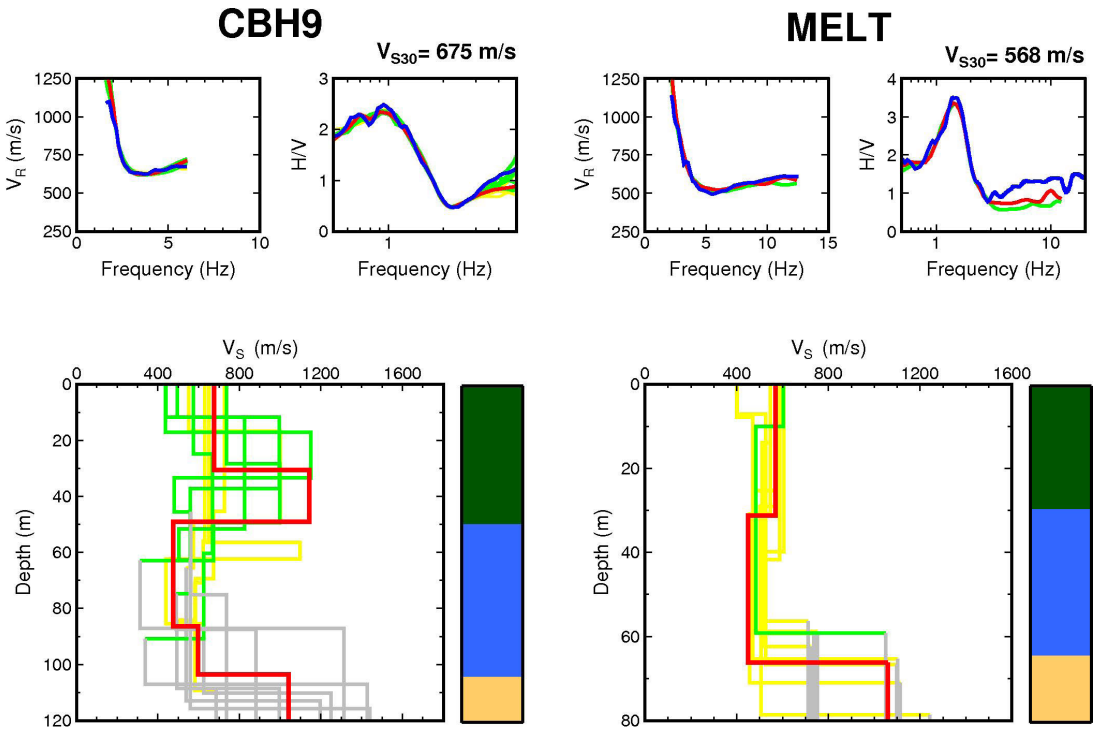

Figure 3. The joint inversion results and stratigraphic interpretation (lower panel) for CBH9 and MELT stations. The best profiles from each of the 10 inversions are shown, with the red profile representing the one with the lowest misfit. The profiles in green are those characterised by a misfit which is within 50% of the best models misfit value; the yellow ones are characterised by a misfit greater than 150% of the best models misfit value. The GL layers are displayed in grey since the values are not reliably constrained by the data. The upper panels show (from left to right) the effective dispersion and H/V curves. The blue curve is the experimental curve, the red curve shows the best fitting theoretical curve while the rest (green and yellow) correspond to the other 9 profiles. The calculated VS30 for each site is displayed in the top right corner. The colours used in the stratigraphic interpretation correspond to the colours in the geological map (Fig. 1).

wave measurements (Farrugia et al., 2016; 2020), the results of which are shown in Fig. 3. It was not possible to obtain shear-wave velocity profiles at the QALA site due to the lack of space in the area to perform ambient noise measurements with the available equipment. However, the presence of a buried clay layer at this site is confirmed through geological mapping and by nearby borehole measurements.

The latest two installed stations are HQIM and XROB, both located in the southern parts of the islands on the GL layer (Agius et al., 2020; Galea et al., 2021). The stations are synchronized using GPS reference time, although this does not affect the spectral shapes. All stations were set to record continuously with a sampling rate of 100 Hz.

With the extension of the Malta Seismic Network to eight stations, three of which are located on UCL, an opportunity to understand the effect of local geology on earthquake ground motion using earthquake data arises. In this study, the data from 2017-2019 is considered. During this time all the three stations installed on UCL were working simultaneously. The HQIM and XROB stations were not used in this study because they were not operative during the study period.

3. Seismogram Analysis

Figures 4 and 5 show the ground acceleration (pseudo-acceleration, after removal of instrument response) of the east-west component of two earthquakes recorded on all the stations of the MSN. The earthquake shown in Fig. 4 has an epicentral distance less than 200 km away from WDD while the earthquake shown in Fig. 5 has an epicentral distance of around 500 km away from the same station. The significant duration (D5-95) was also calculated using OpenSeimsoMatlab (Papazafeiropoulos and Plevris, 2018) and is shown using horizontal bars. This represents the time interval between which 5% and 95% of the seismic energy is attained.

In Fig. 4, amplified ground motion recordings are visible at the MELT and QALA stations with PGA amplification of more than a factor of 3 between QALA, MELT and XLND recordings. The durations ranged between 40.56 s (for XLND site) and 54.62 s (for CBH9 site), with longer durations observed for the CBH9, MELT and QALA sites. These observations can also be done for the earthquake shown in Fig. 5.

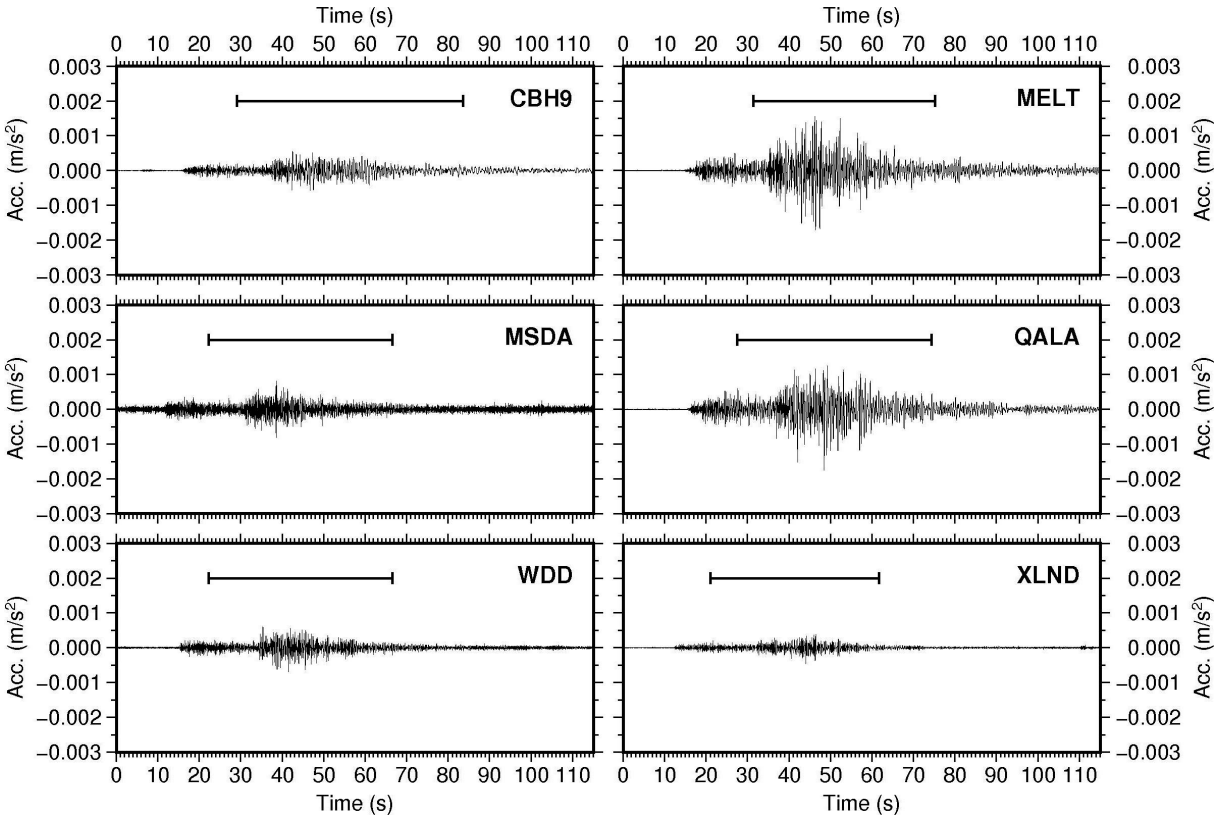

Figure 4. Time series of an earthquake recorded on the MSN stations on 4th August 2018 at 04:07 GMT, magnitude 4.3. The epicentral distance is about 170 km from WDD. The horizontal bars show the significant duration (D5-95).

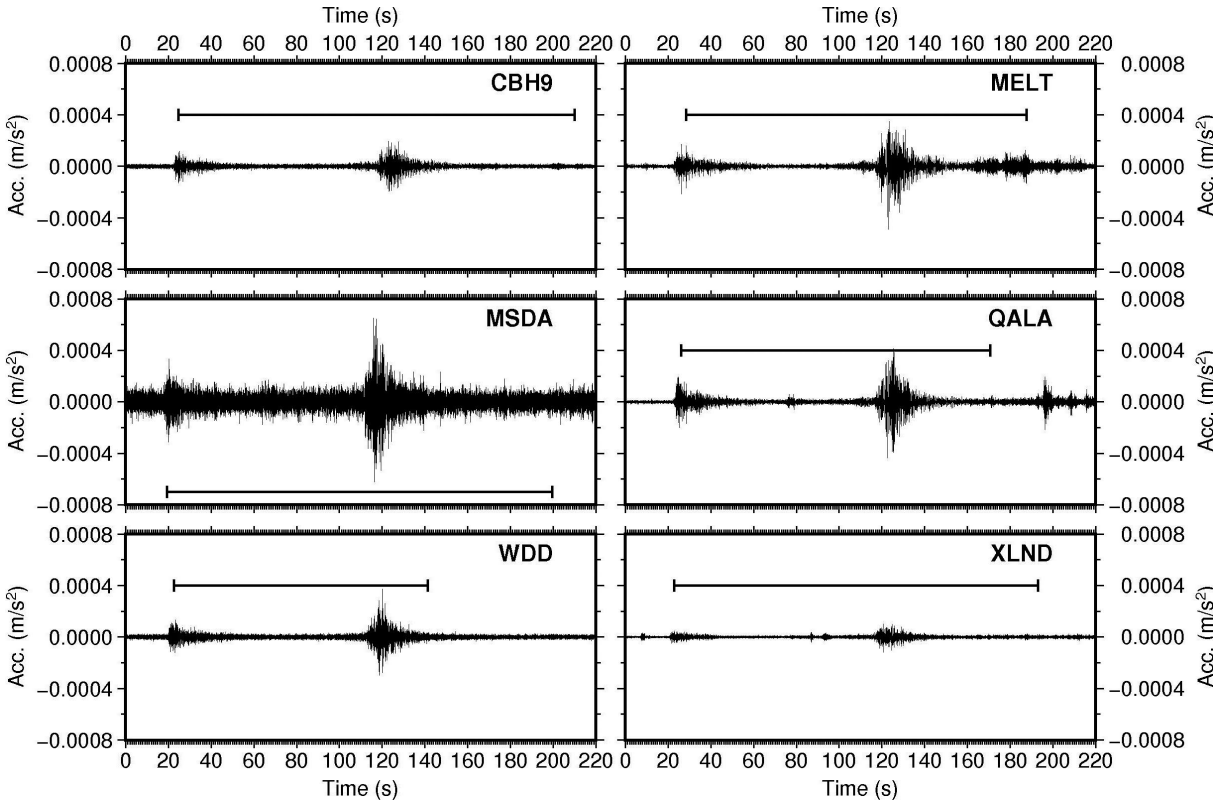

Figure 5. Time series of an earthquake recorded on the MSN stations on 19th August 2018 at 05:48 GMT, magnitude 4.2. The epicentral distance is about 500 km from WDD. The horizontal bars show the significant duration (D5-95).

4. Frequency domain analysis

All the recordings were first checked visually and only those exhibiting a good signal-to-noise ratio, allowing for the detection of the S-wave arrival, were used. Moreover, the earthquakes had to have an epicentral distance to the network of at least five times the interstation distance between the bedrock and study site (12 km) to exclude

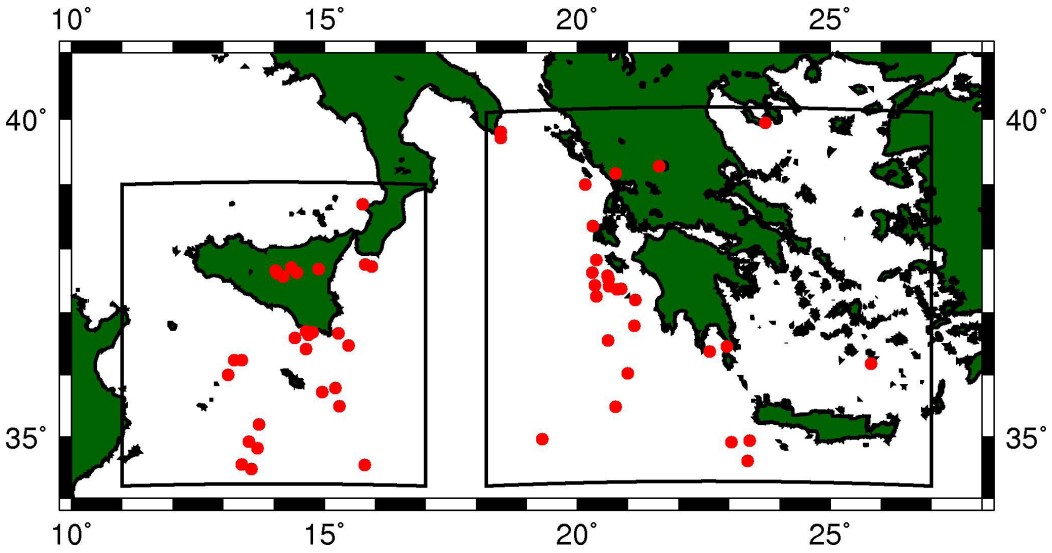

Figure 6. The 58 earthquakes used in the earthquake H/V and SSR techniques. The earthquakes have been divided into 2 sets, as shown in the boxes – near field (eq up to Sicily and S.Italy) and far field (eq along the Hellenic arc, that are generally > 500 km away).

path effects for waves travelling to the stations (Pilz et al., 2009). This resulted in a total of 58 valid earthquakes recorded in the span of 3 years, which are shown in Fig. 6, and listed in Table A1 (appendix).

4.1 Fourier amplitude spectra

Figure 7 shows the Fourier amplitude spectra for the earthquake on 4th August 2018 with an epicentral distance of around 170 km from WDD. Clear amplification in the 1-5 Hz range can be seen for both components (1 horizontal and the vertical) and for both the P- and S-wave, particularly at the MELT and QALA stations. It has to be noted that the S-wave amplitudes are about a factor of 4 higher than the P-wave amplitudes, however the amplification of these sites compared to the other sites is quite significant for the P-wave as well. CBH9, which is also characterised by a buried low-velocity layer, exhibits higher amplitudes for lower frequencies, compared to the other sites, for the S-wave motion. The station with the least overall amplitude is XLND which is known to be directly on Lower Coralline Limestone, however, in general, all the stations installed on both Globigerina Limestone and Lower Coralline Limestone (i.e. no clay is present in the stratigraphy), show low amplitudes.

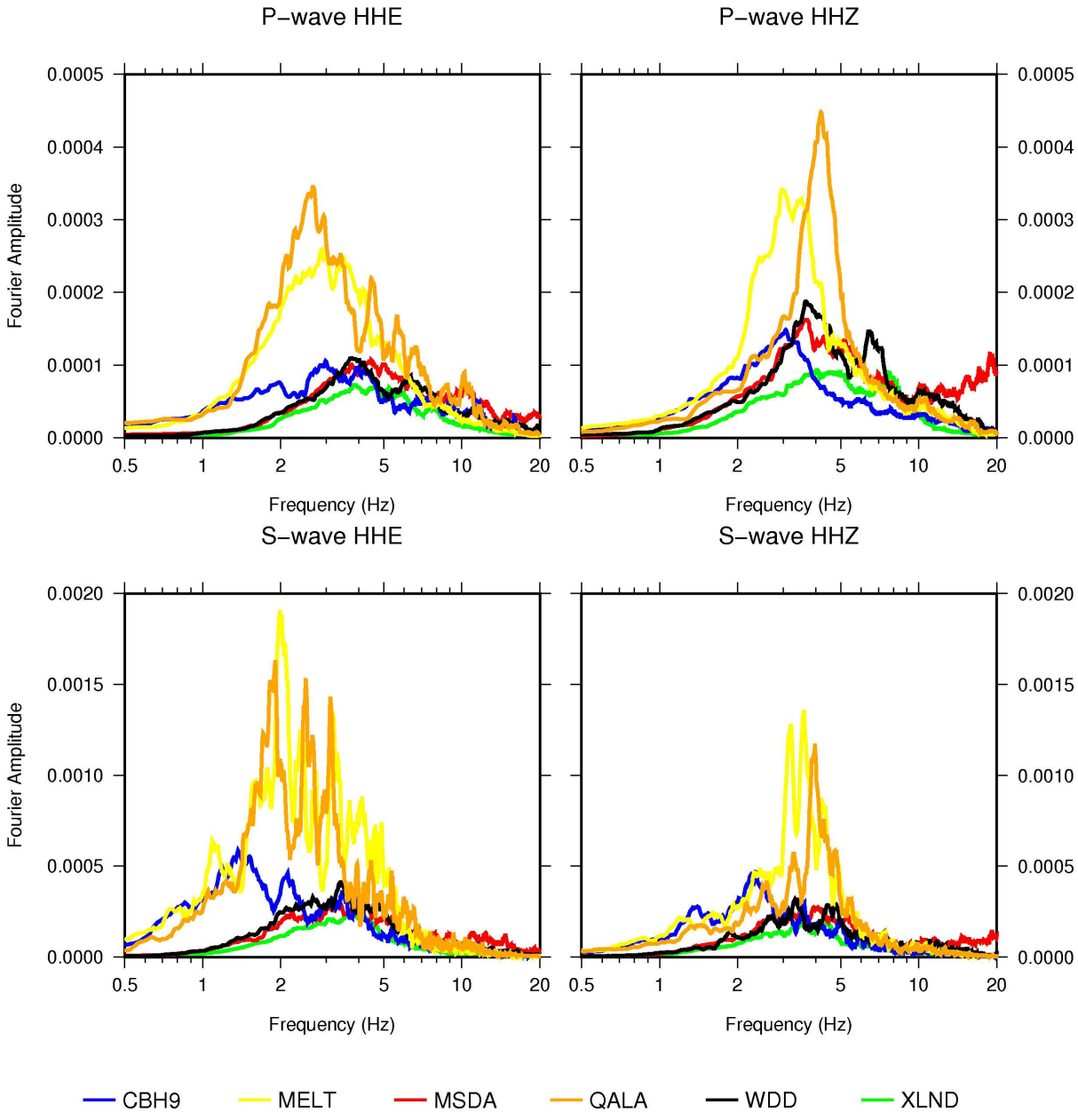

Figure 7. The Fourier amplitude spectra of the all the MSN stations for the earthquake on 4th August shown in Fig. 4.

4.2 Earthquake and noise H/V

The H/V technique was applied to the S-wave portion of suitable local and regional earthquakes recorded on the MSN stations, as well as to a segment of noise recorded on the same stations.

The noise H/V was calculated using 24 hours of data from each station. The recordings were divided into 80 s long windows tapered with a 5% cosine function. This window length can be considered long enough to accomplish the analysis down to a frequency of at least 0.2 Hz. For the earthquake H/V, the time windows for S-waves were first selected, starting 0.7 s before the S-wave arrival and ending when the S-wave energy reaches 90% of its maximum (Pilz et al., 2009). The spectral ratios between the horizontal and vertical components were calculated, and finally, the logarithmic mean of all the H/V ratios was determined for each site.

The noise H/V and earthquake H/V results are presented for each station in Fig. 8. In general, a good agreement can be seen between the curves obtained using noise and earthquake data, with the earthquake H/V curves having slightly higher amplitude than the noise H/V curves.

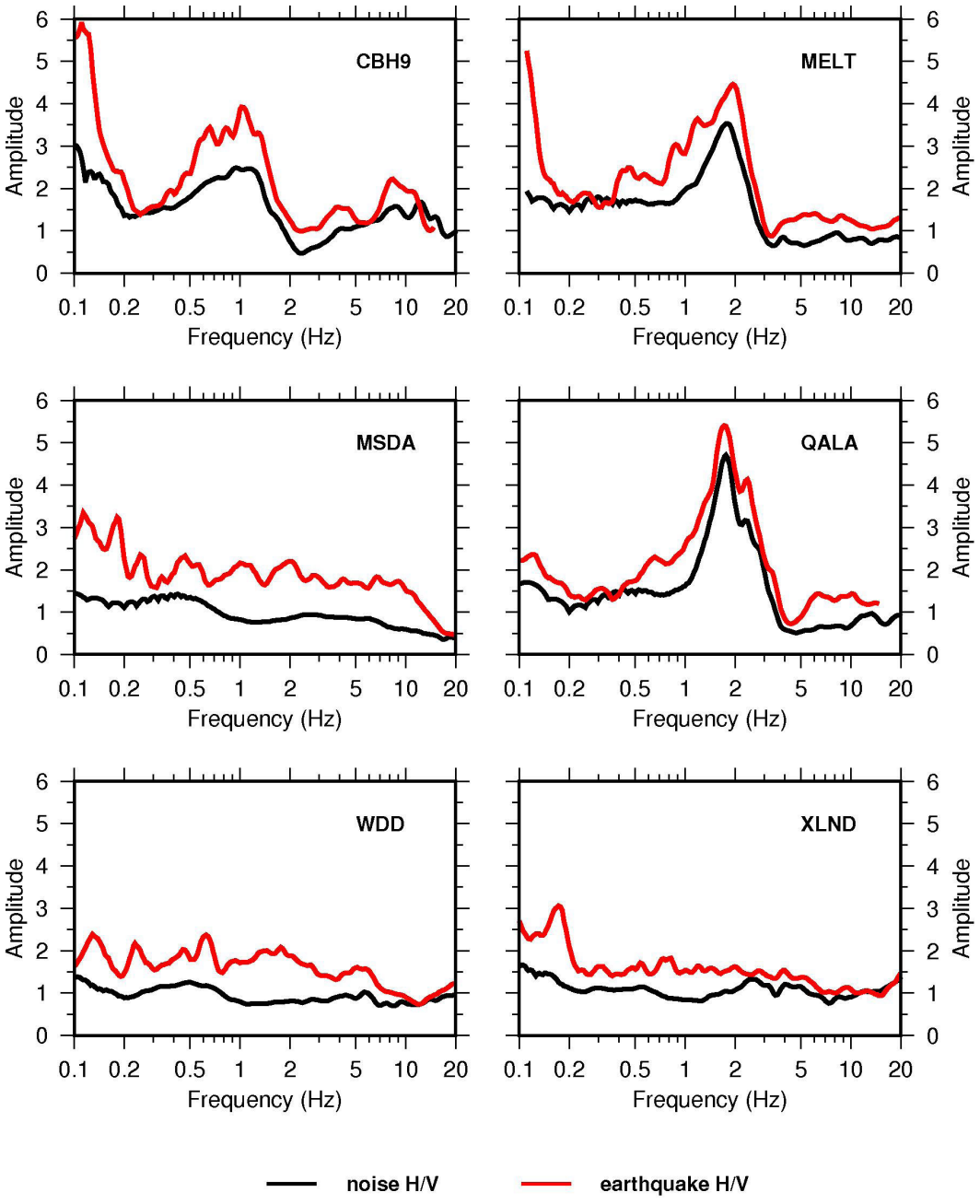

Figure 8. The earthquake H/V (red) and noise H/V (black) curves obtained.

The H/V curves at MSDA, WDD and XLND are generally flat, synonymous with sites on rock, with no significant impedance contrast between different layers. The MELT and QALA curves exhibit a peak close to 2 Hz, which has been consistently obtained at sites with outcropping UCL (Farrugia et al., 2016; Vella et al., 2013) and may be attributed to the impedance contrasts between the clay and underlying/overlying limestone. The peak at CBH9 is significantly broad but within the same frequency range. Such broad peaks may be associated with a dipping impedance contrast (Cornou et al., 2003).

In the curves for MELT and QALA, which are characterised by a buried low-velocity layer, it can be noted that noise H/V dips below 1 for a wide frequency range, a feature which has been observed in various studies (Castellaro and Mulgaria, 2009; Farrugia et al., 2016). This dip, however, is not visible for the H/V curves obtained with earthquake data.

4.3 Standard Spectral Ratio

The Standard Spectral Ratio (SSR) using the S-wave part of the horizontal components was calculated following the method in Pilz et al. (2009). This was conducted for the three stations on UCL (CBH9, MELT and QALA) using the same data set as in the earthquake H/V exercise. The chosen reference station was XLND, since it is the closest to the three stations and also because it is installed on LCL, which can be considered as the bedrock.

The signal was cosine tapered and a Fast Fourier Transformation (FFT) for each horizontal component was performed. Spectral amplitudes were then smoothed using a mean smoothing algorithm, ensuring the preservation of the major features of the earthquake spectra. The two horizontal spectra were averaged for each recording. Finally for each event the spectral ratio between the station on UCL and the XLND station was calculated. The average SSR was then calculated by taking the arithmetic mean of the SSR curves for all earthquakes.

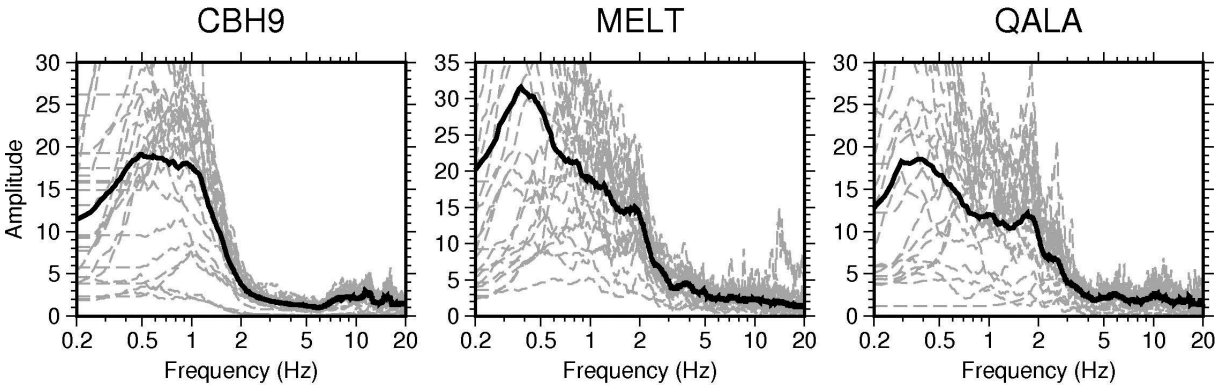

Figure 9. The mean SSR curves, shown in black, obtained for CBH9, MELT and QALA stations, with XLND as the reference bedrock station. The grey curves are the SSR curves obtained for each earthquake.

The three SSR curves (Fig. 9) show significant amplification at frequencies less than 2 Hz, reaching high amplification of more than 30 for the MELT station. The amplification values obtained are outstandingly higher than those obtained using the H/V techniques. This has been noted in various studies such as Pilz et al. (2009) and Parolai et al. (2012).

The SSR curves retain the site resonance frequency shown by the H/V curves, however this frequency is overshadowed for MELT and QALA by the large peaks at around 0.4 Hz. For CBH9, the broad peak between 0.5 and 1.0 Hz is similar to the one exhibited by the H/V curves.

In order to better investigate the reason for the large peaks observed on the SSR at low frequencies, the earthquake sources (shown in Fig. 6) were divided into two categories: near-field earthquakes which span up to Sicily and Southern Italy, and far-field earthquakes which are along the Hellenic arc and are in general more than 500 km away. The SSR procedure was again conducted for these two separate data sets and the results are shown in Fig. 10.

Although the frequency characteristics for the two data sets are similar, we now observe that the far-field earthquakes produce significantly higher amplifications than the near-field earthquakes at frequencies lower than 1 Hz. In particular, the high-amplitude SSR peaks exhibited by MELT and QALA at around 0.4 Hz are visible only in the curves obtained from far-field earthquakes. This is likely to be related to the fact that the far-field earthquakes contain a higher low-frequency content by virtue of their distance and, on average, higher magnitude. Nevertheless it confirms the need for consideration of far-field earthquakes, in particular Hellenic arc earthquakes, in hazard analysis and site amplification at lower frequencies.

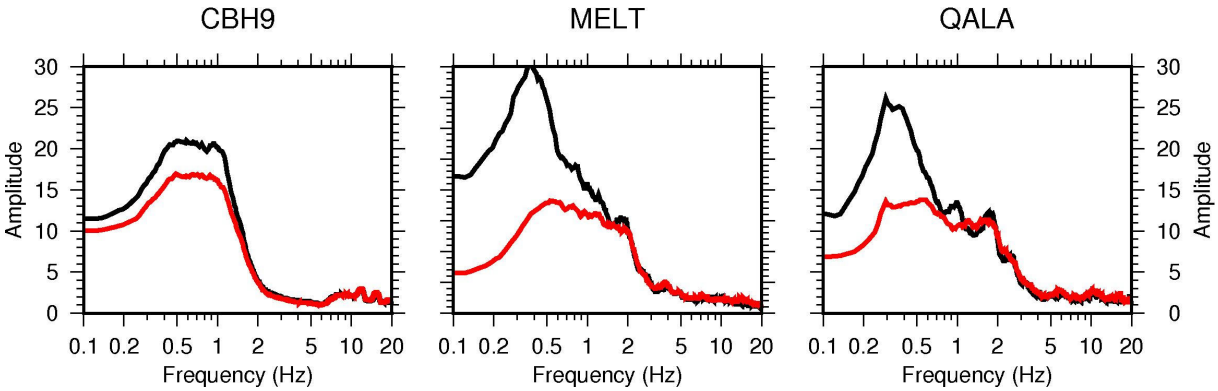

Figure 10. The SSR curves obtained for the near-field (red) and far-field (black) earthquakes.

5. Conclusions

Seismic site effects play an important role in the intensity of an earthquake. This study presents a comprehensive study of site effects at the three sites of the MSN, which are not installed on what is considered as bedrock for the islands. These stations all lie on a layer of limestone which lies on top of a layer of Blue Clay, creating a velocity inversion. Even though in the past decade effort has been made in investigating potential site effects in areas which are characterised by a buried thick low-velocity layer on the islands, this was only done using ambient noise.

This study presents the first national study of site response using earthquake data at the geological site of interest. This was possible with the recent installation of more broadband seismic stations. The data used spanned 3 years (2017-2019). From the seismogram analysis, the potential of amplification at these sites was clearly observed, with amplification reaching a factor of 3 in some cases, and longer durations.

Frequency based analysis was carried out in terms of Fourier amplitude spectra analysis, SSR, earthquake H/V and noise H/V. A significant amplification in the Fourier amplitude spectra for the MELT and QALA sites in the frequency range between 1-5 Hz was observed.

The similarity between the noise and earthquake H/V validates the use of noise H/V technique as a quick method for obtaining the fundamental frequency of a site. As for the SSR results, significantly higher amplifications were obtained when compared to the H/V. An interesting feature only observed on the SSR curves was the high amplification at frequencies lower than what is considered as the resonant frequency of the site for the MELT and QALA stations. By separating the earthquake sources into near- and far-field and repeating the SSR method, it was seen that these peaks can be attributed to distant earthquakes which are richer in low frequency content. The reason for the large amplification at these frequencies, however, needs to be investigated further.

The investigation carried out in this study adds to previous studies in showing that site effects do have a considerable influence on earthquake ground motion at sites characterised by a buried low-velocity layer. Moreover, the SSR technique has revealed important behaviour at lower frequencies which was not previously visible. This has important implications for the response of increasingly common high-rise buildings, and reaffirms the necessity of including such low frequency effects in seismic hazard assessments and building policies.

Data Sharing and Resources. Plots were made using the Generic Mapping Tools version 4.2.1 (www.soest.hawaii.edu/gmt; Wessel and Smith 1998) and SAGA GIS (Conrad et al., 1991-2007).

Acknowledgements. We are grateful to local entities who allowed the use of their premises for the installation of stations (Heritage Malta, Nature Trust, Munxar Local Council, Qala parish, Din l-Art Helwa, Enemed). Funding for stations was provided by Interreg Italia-Malta projects (SIMIT and SIMIT-THARSY, Codes B1-2.19/11 and C1-3.2-57) and by Transport Malta.

References

Bonnefoy-Claudet, S., C. Cornou, P. Y. Bard, F. Cotton et al. (2006). H/V ratio: a tool for site effects evaluation. Results from 1-D noise simulations, Geophys. J. Int. , 167, 827-837, doi:10.1111/j.1365-246X.2006.03154.x.

Bonilla, L. F., J.H. Steidl, G.T. Lindley, A.G. Tumarkin, et al. (1997). Site amplification in the San Fernando Valley, California: Variability of site-effect estimation using the S-wave, coda, and H/V methods, B. Seismolol. Soc. Am. , 87, 3, 710-730, doi:10.1785/BSSA0870030710.

Castellaro, S. and F. Mulargia (2009). The effect of velocity inversions on H/V, Pure Appl. Geophys., 166, 4, 567-592, doi:10.1007/s00024-009-0474-5.

Cornou, C., P.-Y. Bard and M. Dietrich. (2003). Contribution of dense array analysis to the identification and quantification of basin-edge induced waves, Part II: Application to Grenoble basin (French Alps), Bull. Seism. Soc. Am., 93, 6, 2624-2648, doi:10.1785/0120020140.

Dellow, G., Yetton, M. Massey, C. Archibald et al. (2011). Landslides caused by the 22 February 2011 Christchurch earthquake and management of landslide risk in the immediate aftermath, Bull. Nz. Soc. Earthq., 44, 4, 227-238, doi:10.5459/bnzsee.44.4.227-238.

Farrugia, D., E. Paolucci, S. D'Amico and P. Galea. (2016). Inversion of surface wave data for subsurface shear wave velocity profiles characterized by a thick buried low-velocity layer, Geophys. J. Int., 206, 1221-1231, doi:10.1093/gji/ggw204.

Farrugia, D., P. Galea and S. D'Amico. (2020). Modelling and assessment of earthquake ground response in areas characterized by a thick buried low-velocity layer, Natural Hazards, doi:10.1007/s11069-020-04298-w.

Field, E. H. and K. H. Jacob. (1995). A Comparison and Test of Various Site-Response Estimation Techniques, including Three That Are Not Reference-Site Dependent, Bull. Seism. Soc. Am., 85, 1127-1143, doi:10.1785/BSSA0850041127.

Foti, S., S. Parolai, D. Albarello and M. Picozzi (2011). Application of surface-wave methods for seismic site characterization, Surv. Geophys., 32, 6, 777-825, doi:10.1007/s10712-011-9134-2.

Galea, P. (2007). Seismic history of the Maltese islands and considerations on seismic risk, Ann. Geophys., 50, 6, 725-740, doi:10.4401/ag-3053.

Galea, P., M. R. Agius, G. Bozionelos, S. D'Amico et al. (2021). A First National Seismic Network for the Maltese Islands – The Malta Seismic Network, Seismol. Res. Lett., 92, 3, 1-15, doi:10.1785/0220200387.

Lebrun, B., D. Hatzfeld and P.-Y. Bard. (2001). A site effect study in urban area: Experimental results in Grenoble (France), Pure Appl. Geophys., 158, 2543-2557, doi:10.1007/PL00001185.

Nakamura, Y. (1989). A method for dynamic characteristics estimations of subsurface using microtremors on the ground surface, Q. Rep. Railw. Tech. Res. Inst , 30, 1, 25-33.

Mizuno, H. and A. Abe (1991). Site Effects in the Loma Prieta Earthquake and Comparison with an Earthquake Intensity Prediction Method, Proceedings of International Conferences on Recent Advances in Geotechnical Earthquake Engineering and Soil Dynamics, 14, https://scholarsmine.mst.edu/icrageesd/02icrageesd/session13/14/?utm_source=scholarsmine.mst.edu%2Ficrageesd%2F02icrageesd%2Fsession13%2F14&utm_medium=PDF&utm_campaign=PDFCoverPages.

Ohori, M., A. Nobata and K. Wakamatsu (2002). A comparison of ESAC and FK methods of estimating phase velocity using arbitrarily shaped microtremor arrays, Bull. Seismol. Soc. Am., 92, 2323-2332, doi:10.1785/0119980109.

Panzera, F., S. D'Amico, P. Galea, G. Lombardo et al. (2013). Geophysical measurements for site response investigation: preliminary results on the island of Malta, Boll. Geofis. Teor. Appl.,, 54, 111-128, doi:10.4430/bgta0084.

Papazafeiropoulos, G. and V. Plevris (2018). OpenSeismoMatlab: A new open-source software for strong ground motion data processing, Heliyon, 4, 9, 1-39, doi:10.1016/j.heliyon.2018.e00784.

Parolai, S. (2012). Investigation of site response in urban areas by using earthquake data and seismic noise. In: Bormann, P. (Ed.), New Manual of Seismological Observatory Practice 2 (NMSOP-2), Potsdam: Deutsches GeoForschungsZentrum GFZ, 1-38, doi:10.2312/GFZ.NMSOP-2_ch14.

Picozzi, M. and D. Albarello (2007). Combining genetic and linearized algorithms for a two-step joint inversion of Rayleigh wave dispersion and H/V spectral ratio curves, Geophys. J. Int., 169, 189-200, doi:10.1111/j.1365-246X.2006.03282.x.

Pilz, M., S. Parolai, F. Leyton, J. Campos et al. (2009). A comparison of site response techniques using earthquake data and ambient seismic noise analysis in the large urban areas of Santiago de Chile, Geophys. J. Int., 178, 2, 713-728, doi:10.1111/j.1365-246X.2009.04195.x.

Rathje, E. M., M. K. Koçkar and M. C. Özbey (2005). Observed site effects during the 1999 Chi-Chi earthquake and its aftershocks, Seismol. Res. Lett., 76, 2, 238, Abstract.

Ratjhe, E. M., J. P. Stewart, M. Bora Baturay, J. D. Bray et al. (2006). Strong ground motions and damage patterns from the 1999 Duzce earthquake in Turkey, J. Eartq. Eng., Imperial College Press, 10, 5, 693-724, doi:10.1080/13632460609350615.

Riepl, J., P.-Y. Bard, D. Hatzfield, C. Papaioannou et al. (1998). Detailed evolution of site-response estimation methods across and along the Sedimentary Valley of Volvi (EURO-SEISTEST), Bull. Seismol. Soc. Am., 88, 2, 448-502, doi:10.1785/BSSA0880020488.

Takai, N., M. Shigefuji, S. Rajaure, S. Bijukchhen et al. (2016). Strong ground motion in the Kathmandu Valley during the 2015 Gorkha, Nepal, earthquake, Earth Planets Space, 68, 10, 1-8, doi:10.1186/s40623-016-0383-7.

Yamanaka, H. and H. Ishida. (1996). Application of genetic algorithms to an inversion of surface-wave dispersion data, Bull. Seismol. Soc. Am., 86, 436-444, doi:10.1785/BSSA0860020436.

Vella, A., P. Galea and S. D'Amico. (2013). Site frequency response characterisation of the Maltese islands based on ambient noise H/V ratios, Eng. Geol., 163, 89-100, doi:10.1016/j.enggeo.2013.06.006.

***CORRESPONDING AUTHOR: Daniela FARRUGIA**,
Department of Geosciences, University of Malta, Malta
e-mail: daniela.farrugia@um.edu.mt